Ocean Dynamics (2014) 64:1431–1446
DOI 10.1007/s10236-014-0761-2

Methods for estimating the velocities of the Brazil Current in the pre-salt reservoir area off southeast Brazil (23 °S–26 °S)

Tiago Carrilho Biló · Ilson Carlos Almeida da Silveira · Wellington Ceccopieri Belo · Belmiro Mendes de Castro · Alberto Ricardo Piola

Received: 12 May 2014 / Accepted: 30 July 2014 / Published online: 19 August 2014

Abstract The Brazil Current (BC) is likely the least observed and investigated subtropical western boundary current in the world. This study proposes a simple and systematic methodology to estimate quasi-synoptic cross-sectional speeds of the BC within the Santos Basin (23 °S – 26 °S) based on the dynamic method using several combinations of data: Conductivity, temperature, and depth (CTD), temperature profiles, CTD and vessel-mounted Acoustic Doppler Current Profiler (VMADCP), and temperature profiles and VMADCP. All of the geostrophic estimates agree well with lowered Acoustic Doppler Current Profiler (LADCP) velocity observations and yield volume transports of -5.56 ±1.31 and 2.50 ±1.01 Sv for the BC and the Intermediate Western Boundary Current (IWBC), respectively. The LADCP data revealed that the BC flows southwestward and is ∼100 km wide, 500 m deep, and has a volume transport of approximately -5.75 ±1.53 Sv and a maximum speed of 0.59 m s^{-1}. Underneath the BC, the IWBC flows northeastward and has a vertical extent of approximately 1,300 m, a width of ∼60 km, a maximum velocity of ∼0.22 m s^{-1}, and a volume transport of 4.11 ± 2.01 Sv. Our analysis indicates that in the absence of the observed velocities, the isopycnal (σ_0) of 26.82 kg m^{-3} (∼500 dbar) is an adequate level of no motion for use in geostrophic calculations. Additionally, a simple linear relationship between the temperature and the specific volume anomaly can be used for a reliable first estimate of the BC-IWBC system in temperature-only transects.

Keywords Brazil Current · Intermediate Western Boundary Current · Santos Basin circulation · Geostrophic estimates

Responsible Editor: Pierre De Mey

T. C. Biló (✉) · I. C. A. da Silveira · B. M. de Castro
Instituto Oceanográfico da Universidade de São Paulo, São Paulo, Brasil
e-mail: tiago.bilo@usp.br

W. C. Belo
Centro de Pesquisas e Desenvolvimento Leopoldo A. Miguez de Mello, Petróleo Brasileiro, SA, Brasil

A. R. Piola
Sección Dinámica Oceánica, Servicio de Hidrografia Naval (SHN), Universidad de Buenos Aires, and Instituto Franco-Argentino sobre Estudios de Clima y sus Impactos, CONICET, Buenos Aires, Argentina

1 Introduction

The exploration and environmental control of the recently discovered giant oil and gas reservoirs within the Santos Basin (23 °S – 28 °S, Fig. 1), also referred as Santos Plateau area in the oceanographic literature, have brought new demands for operational oceanography, including improved knowledge of the ocean circulation in Brazilian territorial waters. These reservoirs (pre-salt reservoirs) are located in an oceanic region that is typically deeper than 1,000 m and are the result of the deposition of organic matter in microbial carbonates (or microbialites). These organic deposits preceded the deposition of a thick-salt layer, which marks the Aptian during the opening of the Atlantic Ocean approximately 120 million years ago (Meisling et al. 2001; Duarte and Viana 2007; Carminatti et al. 2008; Mohriak et al. 2010). The salt deposits drastically modified the geomorphological profile of the Brazilian continental margin and formed the São Paulo Plateau (3,000–3,600 m), which reduced the steepness of the continental slope and

replaced the continental rise within the Santos Basin (Zembruscki 1979).

The technological demands of oil and gas exploration at depths of 1,000 to 3,500 m require adequate knowledge and monitoring of surface waves and ocean currents. The temporal and spatial variabilities of the western boundary jets also need to be understood and monitored. Some of this information can be obtained from satellite observations, but the use of such images can only provide either surface (via Synthetic Aperture Radar (SAR)) or depth-integrated (through altimetry) estimates of the circulation. In situ observations are thus required to vertically extend and increase the level of detail of the characterization of these currents.

In contrast to these operational requirements, the Brazil Current (BC) is likely the least observed and investigated subtropical western boundary currents in the world. Consequently, the BC's mean flow and its variability are poorly understood. The presence of operational, geophysical, and oceanographic vessels in the Santos Basin represent a unique opportunity to broaden the observational base of the BC and its associated mesoscale activity, which in turn can positively impact the exploration and production of the "Pre-Salt" reservoirs. Repeated hydro-oceanographic transects will be performed by ships involved in both oil and gas exploration and environmental monitoring operations. Hence, ships equipped with different oceanographic instruments will allow monitoring of the BC at rates that have not been available previously.

This work proposes a systematic methodology to estimate quasi-synoptic cross-sectional speeds of the BC within the Santos Basin for cases in which data are acquired by (i) a vessel-mounted Acoustic Doppler Current Profiler (VMADCP) and conductivity–temperature–depth (CTD) profiling, (ii) VMADCP and temperature profiling, (iii) only CTD profiling, and (iv) only temperature profiling. These estimates are based on the application of the dynamic method to calculate geostrophic velocities.

2 Western Boundary Current Patterns in the Santos Basin

Most of the available information about the surface speeds and volume transport for the BC is based on geostrophic calculations using the classical dynamic (geostrophic) method referenced to an arbitrarily chosen level of no motion. The BC surface speeds range from -0.3 to -0.85 m s^{-1} (where negative indicates poleward currents), and the volume transport varies from -5 to -16 Sv (1 Sv = 10^6 m^3 s^{-1}) (Signorini 1978; Miranda and Filho 1979; Evans et al. 1983; Stramma 1989; Garfield 1990; Campos et al. 1995; Lima 1997; Silveira et al. 2001). It is difficult to compare the results from these studies because they employed different zero cross-section velocity levels, ranging from 500 to 1,300 m, in their geostrophic computations. In some calculations, the BC is assumed to transport only Tropical Water (TW) and South Atlantic Central Water (SACW) and, therefore, to only occupy the upper 500 m of the water column (Stramma and England 1999). Other authors assumed that the BC carries TW, SACW, Antarctic Intermediate Water (AAIW), and Upper Circumpolar Deep Water (UCDW) (Mémery et al. 2000) and thus assumed that the BC extends to a depth of 1,300 m.

The choice of the appropriate level of no motion to better reproduce the speeds, geometry, and transport of the BC using the dynamic method should be addressed based on directly measured velocity profiles. Within the Santos Basin, only three studies provide such information: (Evans and Signorini 1985); (Müller et al. 1998); (Rocha et al. 2014). Evans and Signorini (1985) presented a cross-isobath series of quasi-synoptic profiles at approximately 23 °S, which revealed that the BC extends to depths of 400–500 m and that a counterflow is present underneath to a maximum depth of 800–900 m. On the other hand, Müller et al. (1998) described the results of a currentmeter mooring line located at 28 °S that indicated that the BC extends to a depth of approximately 1,300–1,500 m. Rocha et al. (2014) presented an analysis of a 12-month time series from a currentmeter mooring deployed at 25 °S that indicated that the velocity pattern at this latitude resembles that reported by Evans and Signorini (1985) .

The answer to this apparent dichotomy in the vertical extent of the BC was provided by Boebel et al. (1999), who performed an analysis of trajectories of Lagrangian floats and explained that both the AAIW and UCDW reach the South American continental margin from the east as part of the intermediate-upper deep parts of the South Atlantic Subtropical Gyre. The AAIW/UCDW flow splits into two branches as it hits the southern portion of the Santos Basin. This flow split was named by the authors as the Santos Bifurcation; one branch turns poleward, and the other goes through a cyclonic loop before turning toward the equator (Fig. 1). The axis of the Santos Bifurcation is located at approximately 27 °S (Legeais et al. 2013). The northward-flowing branch of the AAIW/UCDW organizes itself as a narrow elliptically-shaped undercurrent that is commonly referred to as the Intermediate Western Boundary Current (IWBC). This undercurrent flowing opposite to the BC imposes a quiescent level at approximately 500 dbar.

While the appropriate choice of the level of no motion is apparently immediate upon examining the literature, there is no quantitative assessment of whether the geostrophic velocity estimates referenced to 500 dbar are good proxies for the observed meandering BC flow and therefore if those estimates can reproduce the appropriate partition between the barotropic and baroclinic components of the BC. We

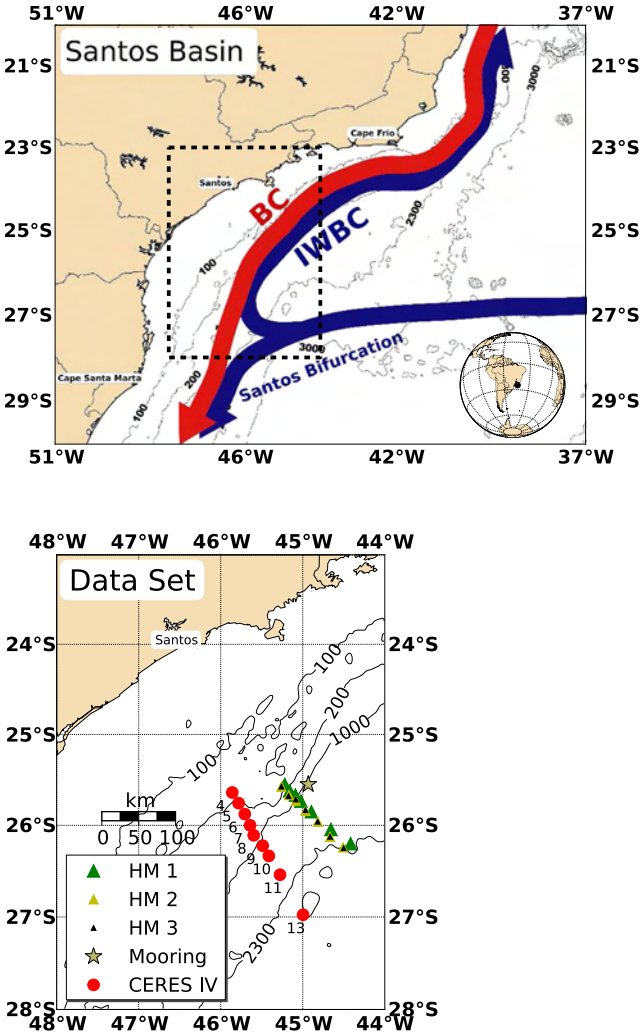

Fig. 1 Schematics of the Brazil Current (BC), the Intermediate Western Boundary Current (IWBC) and the Santos Bifurcation flow pattern based on Boebel et al. (1999) and Legeais et al. (2013) (upper panel). The *dashed box* indicates the area shown in detail in the lower panel. The *circles* represent the locations of the CTD/LADCP stations of the CERES Experiment cruise. The location of the COROAS mooring is represented by the star, and the *triangles* indicate the locations of the CTD stations of the COROAS transect

also test how the different geostrophic velocity estimates compare to the currents that have been observed from top–bottom profiling by Lowered-ADCP (LADCP). We make theses comparisons by focusing on the BC at 26 °S.

3 Data and methods

3.1 The data set

Two data sets are used in this work. The first is a historical data set from the COROAS experiment, which was the Brazilian component of the World Ocean Circulation Experiment (WOCE) (Campos et al. 1996). This data set consists of a four-level currentmeter mooring and a repeated quasi-synoptic hydrographic transect off the city of Santos (Fig. 1). The mooring was deployed over the 1,000 m isobath (25.55 °S, 44.93 °W) approximately 17 km from the transect, and the currentmeters were placed at depths of 29, 91, 293, and 698 m. The time series extend from 21 December 1992 to 20 March 1994. The hydrographic transect was repeated during the HM 1 (January 20, 1993–February 03, 1993), HM 2 (July 17, 1993–July 29, 1993) and HM 3 (January 20, 1994–January 19, 1994) cruises.

The second data set is part of the CERES experiment, which consisted of five quasi-synoptic hydrographic surveys to investigate the BC and its recirculation cells within the pre-salt reservoir area. Here, we analyze one transect from the fourth cruise (June 2010), which consisted of simultaneous top–bottom CTD and LADCP profiling. The locations of the CERES experiment stations are shown in Fig. 1. Underway, continuous 75 kHz VMADCP observations from the surface to approximately 300 m was also obtained.

The data sets are used in this study as follows. In Section 4, the COROAS currentmeter mooring and hydrographic transects are used to evaluate how the zero cross-section velocity level changes with time and how applicable the 500 dbar average level of no motion is to the temporally-evolving BC. In Section 5, we compare the observed top–bottom velocity patterns with the geostrophic estimates considering the different data sources that are available, as was discussed in Section 1.

3.2 Methods

3.2.1 Processing of the COROAS mooring data

Each currentmeter time series was low-pass filtered using a Lanczos squared filter with a 40h cut-off (e.g., Emery and Thomson 2001 to primarily retain the subinertial oscillations. The inertial period at the mooring location is 27.74 h. The daily averaged velocity vectors are presented in a Cartesian coordinate system that is rotated 45° clockwise so the x-axis and y-axis are the along and normal directions to the COROAS hydrographic transect, respectively (Fig. 2).

We then follow Silveira et al. (2008) and Rocha et al. (2014) in interpolating the four instrument levels to obtain a smoothed profile of the horizontal velocity and to infer the velocity inversion depth (i.e., the zero cross-section velocity level). The method consists of projecting the discrete velocity values at the currentmeter depths onto the quasi-geostrophic dynamic modes of the vertical structure (the barotropic and the first three baroclinc modes). We computed the dynamic modes using a mean stratification frequency profile $N^2(z)$ calculated from the World Ocean Atlas 2013 (WOA13) climatology. The 117

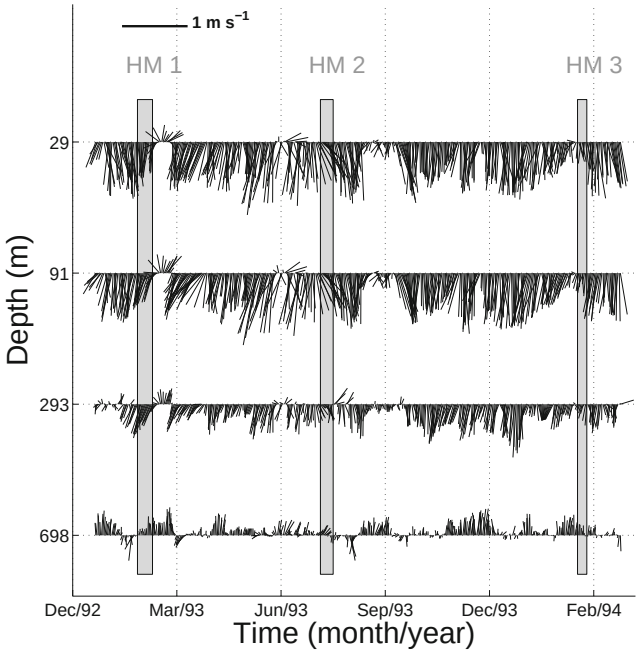

Fig. 2 Low-passed filtered and rotated current time series for the 29, 91, 293, and 698 m levels of the COROAS mooring (25.55 °S, 44.93 °W). The scaling vector of 1.0 m s^{-1} is oriented along the COROAS transect shown in Fig. 1. The *shaded bars* denote the periods during which the COROAS hydrographic surveys were conducted

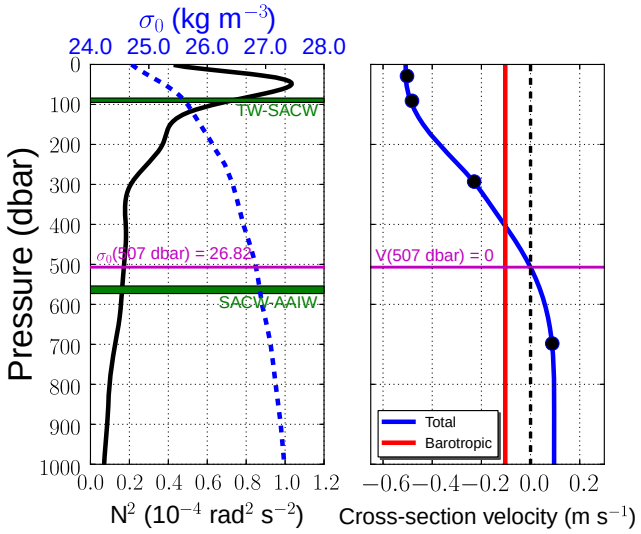

Fig. 3 Climatological $N^2(z)$ and σ_0 profiles (left panel), and the vertical profile of the mean cross-section velocity (right panel) at 25.55 °S, 44.93 °W. The *shaded green* regions correspond to the TW-SACW and SACW-AAIW interfaces from Mémery et al. (2000). The *black dots* mark the four discrete mean currentmeter values at the currentmeter depths. The *red line* represents the mean barotropic velocity component, and the *magenta line* indicates the depth of the mean zero cross-section velocity level

climatological temperature (Locarnini et al. 2013) and salinity (Zweng et al. 2013) profiles over the continental slope (23 °S–26 °S) were averaged to generate the potential density $\sigma_0(z)$ and $N^2(z)$ profiles (Fig. 3, left panel).

3.2.2 The dynamic method

The geostrophic estimates carried out in this work are based on the classic dynamic method expression given by Eq. 1.

$$v(p) = v_r + \frac{1}{f_0}\int_p^{p_r} \frac{\partial \delta}{\partial x} dp', \tag{1}$$

where $v(p)$ is the cross-sectional velocity at the pressure level p, v_r is the known velocity at the reference isobaric level p_r [$v_r = v(p_r)$], δ is the specific volume anomaly, f_0 is the Coriolis parameter, and x is the along-section coordinate. The variations in how to apply Eq. 1 are based on how to identify or define v_r and/or to obtain δ within the Santos Basin.

3.2.3 LADCP and VMADCP data processing

During the CERES experiment, velocity profiles were obtained using a downward-looking 300 kHz LADCP Workhorse Sentinel from RD Instruments. The average velocity profile at each station was calculated following the procedures described by Fischer and Visbeck (1993) and Visbeck (2002). The ocean velocities in the first 400 m, which were measured simultaneously by a 75 KHz VMADCP Ocean Surveyor (also from RD Instruments), were included in the LADCP data processing to additionally constrain the solution of the inverse problem. This methodology reduces errors because the constraints from bottom tracking and the upper ocean velocities force the average velocity profile to agree with these more accurate data (e.g., Visbeck, 2002, Schott et al. 2005). The VMADCP data processing was conducted using the processing software Common Ocean Data Access System (CODAS) from the Currents Group of the University of Hawaii.

4 COROAS mooring and hydrographic transects

4.1 COROAS mooring

The filtered and rotated velocity time series of the four measured levels of the COROAS Mooring are presented in Fig. 2. The upper three levels are clearly within the BC domain due to the generally southwestward flow direction. The speed near the surface reaches 1.10 m s^{-1}, but its mean value is 0.55 m s^{-1} with a standard deviation of 0.23 m s^{-1}. The velocity decays monotonically with depth within the BC. Significant and vertically-coherent variability is observed in the three upper levels, but only four events

of flow reversal are observed during the 15 months of the series. This differs from the BC activity reported by Silveira et al. (2008) and Rocha et al. (2014) near Cape Séo Tomé (22 °S) and Cape Frio (23 °S), where longer and more frequent flow reversals were reported. The currentmeter at the deepest level is within the IWBC and shows a mean speed of 0.12 m s^{-1} to the northeast and a standard deviation of 0.09 m s^{-1}. The maximum observed IWBC speed is 0.45 m s^{-1}.

The modal projection procedure described in Section 3.2.1 was performed at each time step of the time series to obtain the velocity profile time series. Because we want to evaluate both the mean velocity profile and the time dependency of the zero cross-section velocity level, we computed the average velocity profile over the mooring period (Fig. 3, right panel) and identified the level of no motion at each time step. This mean velocity profile has maximum southwestward velocities of -0.55 m s^{-1} and northeastward velocities of 0.12 m s^{-1}, as was described above. Figure 4 illustrates the time series of the level of zero cross-section velocity at the profiles that contain velocity inversions. The level of no motion oscillates around 500 dbar with a mean value of 507 dbar and a standard deviation of 131 dbar.

Because we also wish to relate the zero cross-section velocity level to the interfaces between the water masses in the Santos Basin, we used the isopycnal interfaces estimated by Mémery et al. (2000). These density values were converted to $\sigma_0(z)$, and we searched for the pressure levels at which they occur in the climatological $\sigma_0(z)$ profile (Fig. 3, left panel). The depth ranges of the water mass interfaces are presented in Table 1.

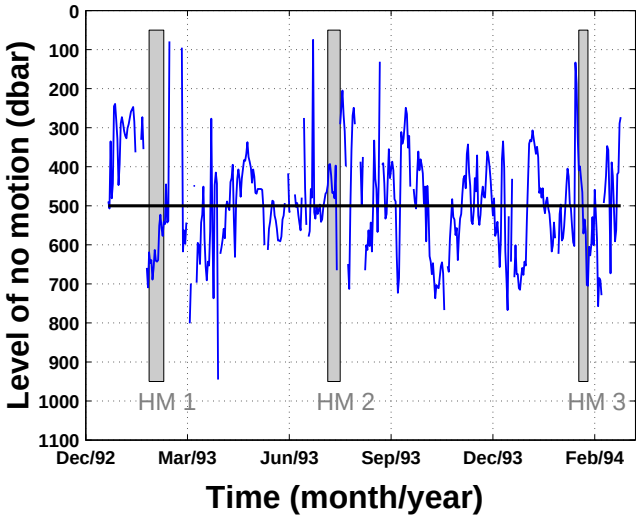

Fig. 4 Time series of the zero cross-section velocity level estimated from the COROAS currentmeter data. The *horizontal solid line* shows the mean value of the time series (507 dbar). The *shaded bars* denote the periods during which the COROAS hydrographic surveys were conducted. The mooring was deployed over the 1,000 m (∼1,009.20 dbar) isobath

Figure 3 (right panel) depicts the average BC-IWBC system that is described above. As pointed out by Rocha et al. (2014), the barotropic velocity component is approximately -0.1 m s^{-1} over the 1,000 m isobath. The panels from Fig. 3 illustrate the relationship between the water mass and velocity pattern that is described in the literature. The level of no motion is similar to the SACW-AAIW interface from Mémery et al. (2000) (within ∼50 dbar), which indicates that this interface level represents the transition depth between the BC and the IWBC within the Santos Basin.

4.2 Hydrographic transects

To evaluate whether the SACW-AAIW interface is a suitable level of no motion, we carried out geostrophic estimates (Eq. 1) from the COROAS repeated quasi-synoptic hydrographic transect. The geostrophic velocities are computed relative to the isopycnal level of no motion (e.g., Stramma et al. 1995). The climatological isopycnal level (26.82 kg m^{-3}) at the corresponding no motion pressure level (507 dbar) observed in the mooring is used as reference (see Fig. 3). All of the hydrographic transects also showed the 26.82 kg m^{-3} isopycnal at a mean level of approximately 500 dbar. This method represents a rough and simple assessment of the BC system that does not require shoreward extrapolations of the mass field, although the transports and a comparison between the geostrophic estimates and the mooring data can indicate whether 500 dbar is an appropriate reference level.

The BC and IWBC transports were computed using the well-defined areas of the velocity cores presented in Figs. 5, 6, and 7. Following Rocha et al. (2014), the RMS differences between the geostrophic profiles closest to the mooring location at each transect and the cruise-period average velocity profile from the mooring were also computed. The HM 1 transect (Fig. 5) shows that the BC flows southwestward with a maximum velocity of approximately -0.40 m s^{-1} and a transport of -3.59 Sv. The IWBC is depicted as a northeastward flow with a maximum velocity of ∼0.23 m s^{-1} and a transport of 2.35 Sv, and its core is located directly beneath the BC's core. The geostrophic velocity profile at the mooring location accurately represents the velocity structure from the mooring observations

Table 1 Pressure levels of the water mass interfaces from Mémery et al. (2000) on the continental slope of the study region (23 °S–26 °S)

	TW-SACW	SACW-AAIW
σ_0 (kg m^{-3})	25.60 ± 0.03	26.90 ± 0.01
Pressure range (dbar)	89 ± 6	563 ± 10

The pressure ranges correspond to the 95 % confidence intervals

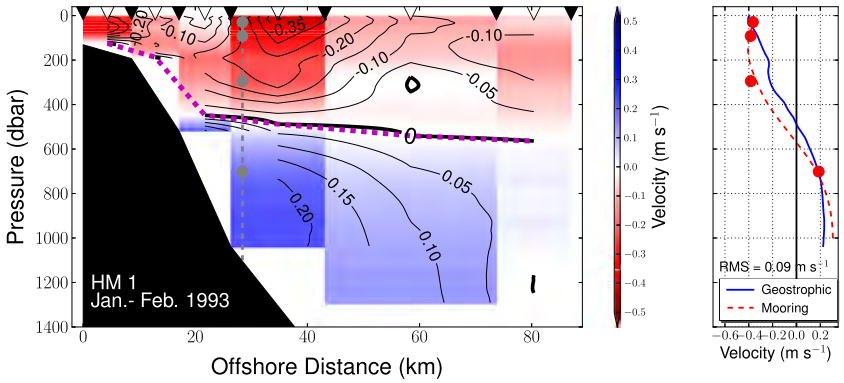

Fig. 5 **a** Geostrophic velocity for the HM 1 transect referenced at the 26.82 kg m^{-3} isopycnal level (*magenta line*) and **b** comparison of the geostrophic velocity profile and mooring velocity (time-averaged over the period of the cruise). *Black triangles* represent the hydrographic stations, and the *white triangles* represent the positions of the geostrophic velocity profiles. The *gray line and markers* represent the positions (along-section) of the mooring and the instrument pressure levels, respectively

with a RMS of 0.09 m s^{-1}. The main difference is the sharper decay of the geostrophic velocity with depth in the BC domain.

The HM 2 transect (Fig. 6) shows that the BC has a maximum surface velocity of -0.8 m s^{-1} and a volume transport of -6.71 Sv. The IWBC has a maximum velocity approximately 0.13 m s^{-1} and a transport of 2.96 Sv. Note that the BC and IWBC cores are not aligned along the x-axis as in the HM 1 transect. Both sections show the IWBC core at ∼900 dbar, but the IWBC is displaced offshore from the BC core in the HM 2 transect. This pattern is also suggested by the currentmeter data (Fig. 6, right panel). The geostrophic velocity profile at the mooring location represents the mooring profile fairly well; the RMS between them is 0.08 m s^{-1}.

Finally, the HM 3 transect is presented in Fig. 7. Unlike the situations observed in Figs. 5 and 6, the HM3 cruise shows a very weak cross-section BC-IWBC system. The BC core has maximum velocities of approximately -0.22 m s^{-1} at subsurface levels (∼50 dbar) and a volume transport of -1.50 Sv. At intermediate levels (800-1,000 dbar), the IWBC core has maximum velocities of ∼0.12 m s^{-1} and a transport of 0.24 Sv. Offshore from the IWBC, there is a southwestward flow with velocities of less than 0.06 m s^{-1}. Note that in the right panel of Fig. 7, the geostrophic velocity profile at the mooring site has a similar flow pattern to the mooring profile, yielding a RMS of 0.09 m s^{-1}. The low cross-sectional BC velocities may be related to its meandering activity (e.g., Rocha et al. 2014).

The cruise periods analyzed here illustrate three distinct situations of the BC in terms of the speed (corroborated by the mooring observations) and, consequently, volume transports. Campos et al. (1995) and Rocha et al. (2014) found that the BC flows southwestward transporting approximately -5.7 Sv in the same region. We found a comparable value only in the HM 2 transect (-6.71 Sv); however, the deeper reference levels (750 and 900 dbar) used by Campos et al. (1995) overestimated the BC's vertical extent, and no IWBC was observed.

In the IWBC domain, the HM 1 and HM 2 transects show intermediate flows that are consistent with those found in the literature; the core is close to the continental slope, the maximum velocities range from 0.13 to 0.23 m s^{-1}, and the current reaches depths greater than 1,500 dbar (e.g., Evans and Signorini 1985; Silveira and

Fig. 6 Similar to Fig. 5 but for the HM 2 transect

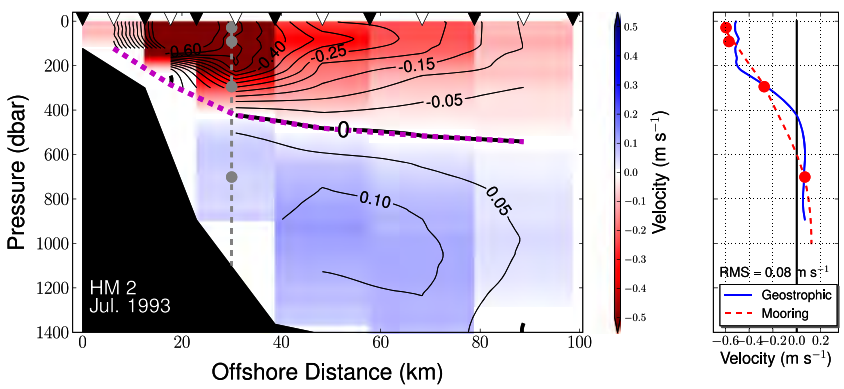

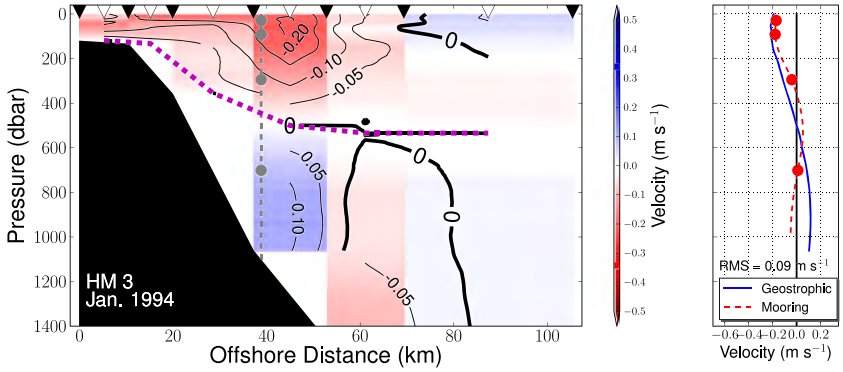

Fig. 7 Similar to Fig. 5 but for the HM 3 transect

Calado 2004; Legeais et al. 2013; Rocha et al. 2014). However, the distinct scenario presented in the HM 3 transect, which is corroborated by the mooring data, suggests a possible perturbed state of the IWBC. The float trajectories presented by Legeais et al. (2013) also show such activity suggesting the presence of meanders and water recirculation.

5 The CERES IV quasi-synoptic survey

In the previous section, we showed the applicability of the 26.82 kg m^{-3} (∼500 dbar) isopycnal level as the reference depth for geostrophic calculations within the Santos Basin (23 °S–26 °S) and described the mean velocity profile off the city of Santos. Oceanographic vessels are commonly equipped with VMADCPs, which can provide a good estimate of v_r in Eq.1 (e.g., Pickart and Lindstrom 1994; Campos et al. 1996; Meinen et al. 2000).

In this section, we test two approaches for determining the reference speeds and compare them to top–bottom observed sectional velocity patterns. Geostrophic estimates are calculated considering the following data sources: (i) VMADCP and CTD profiles, (ii) VMADCP and temperature profiles, (iii) only CTD profiles, and (iv) only temperature profiles. We used the CERES experiment data set to perform these study cases.

5.1 Section of LADCP-measured velocity

As described before, the top–bottom observed velocity profiles are from the LADCP transect. The observed cross-sectional velocity field is shown in Fig. 8 (upper panel). Note that the BC flows to the southwest in the upper 500 dbar with maximum surface velocities of approximately -0.59 m s^{-1} and a width of ∼100 km. The parabolic-shaped current is centered over the 630 m isobath (station 8) and is well defined between stations 6 and 11.

At station 13, a northeastward flow with velocities of approximately 0.03–0.05 m s^{-1} is observed near surface. This flow may be related to a BC recirculation cell. Because there is no clear evidence of a recirculation at 26 °S–25 °S and at this offshore distance (e.g., Vianna and Menezes 2011), further investigation of this velocity signal is required.

At intermediate depths, the IWBC is depicted as flowing northeastward with a maximum velocity of approximately 0.22 m s^{-1} and a vertical extent between 500 and 1,800 dbar. Because of the large distance between stations 11 and 13 (56 km), it was not possible to define the IWBC's horizontal dimension, but its signal is well defined between stations 8 and 11, indicating a minimum width of ∼60 km. This value is consistent with the geostrophic estimates from our HM COROAS transects and the width of ∼60 km presented by Silveira et al. (2004) from Pegasus profiling at 23 °S. The IWBC's core is displaced approximately 30 km offshore (station 10) from the BC core.

After defining the dimensions of the BC and IWBC, we computed their volume transports by integrating the cross-sectional velocities over the area covered by each current. We also integrated the LADCP accuracy of 0.05 m s^{-1} over the same areas that were used to compute the transports to estimate the transport error. We estimated the BC and IWBC transports as -5.75 ± 1.53 and 4.11 ± 2.01 Sv, respectively. We also computed the observed barotropic velocity field from the mean velocity of each profile (Fig. 8, lower panel). Considering the same area that was used to compute the total BC transport, the estimated barotropic transport was -2.30 Sv, which corresponds to ∼40 % of the total.

Finally, note that there is a well-defined deep southwestward flow at the easternmost stations (11 and 13) with maximum velocities of approximately 0.15 m s^{-1} at ∼1700 dbar at station 13 (Fig. 8, upper panel). Currentmeter records (Müller et al. 1998) have indicated that over the ∼2,200 m isobath at 23 °S and 28 °S, there is a poleward, weak, and highly variable flow (∼-0.5 ±0.15 m s^{-1}) at depths greater than 1,900 m that is related to the North Atlantic Deep Water (NADW) circulation. Recently, Meinen et al. (2012) presented results from a pressure-equipped inverted

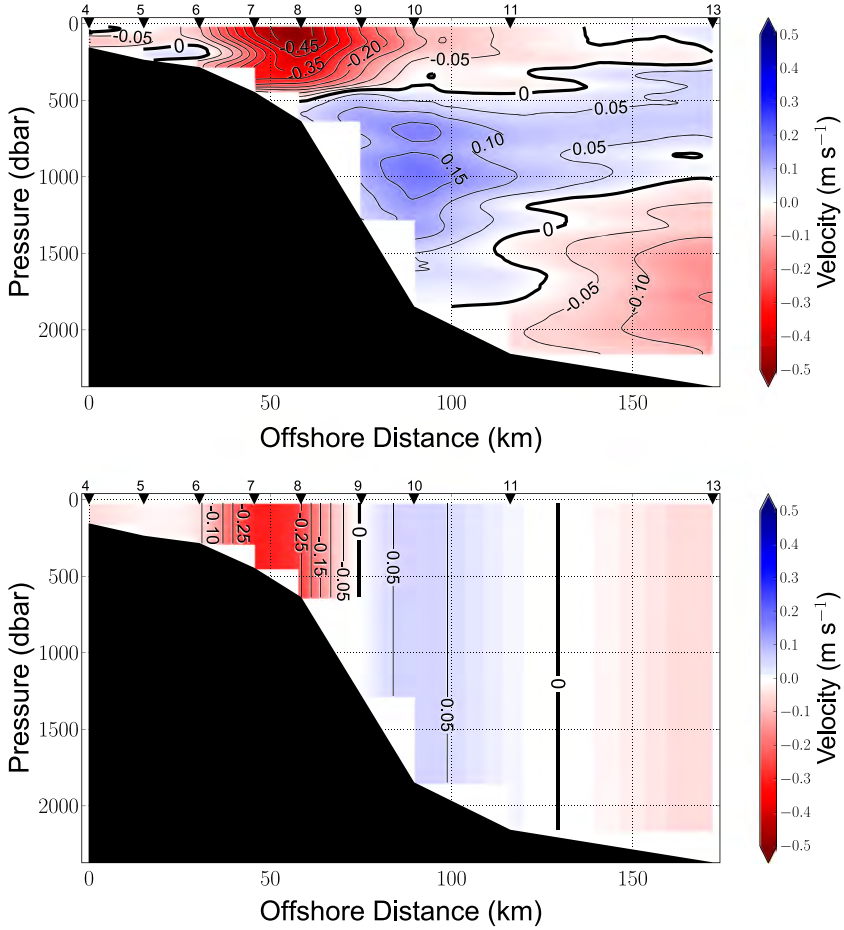

Fig. 8 Cross-sectional velocity transect measured by LADCP (*upper panel*) and its corresponding barotropic component (*lower panel*). Negative velocities are southwestward, and the *triangles* indicate the locations of the stations

echo sounder array at 34.5 °S that revealed a weak but well-organized poleward NADW flow associated with the Deep Western Boundary Current (DWBC). Thus, to verify if we observed the DWBC signal at stations 11 and 13, we performed a simple water mass analysis.

The TS diagram and the potential temperature and salinity transects overlaid on Mémery et al. (2000) water mass interfaces (Fig. 9) show the presence of five typical mid-latitude water masses in the South Atlantic: TW, SACW, AAIW, UCDW, and NADW. Combining the sectional distribution of the water masses together with the velocity section clearly illustrates the known western boundary circulation within the Santos Basin. The TW and SACW follow the path of the BC in the upper 500 dbar, and the AAIW and UCDW are advected by the IWBC at intermediate depths.

Using the water mass interfaces proposed by Mémery et al. (2000), the NADW was found to be deeper than 1,500 dbar at stations 10, 11, and 13. This indicates that the southwestward flow observed in the LADCP data may be part of the DWBC. In addition, we tested the NADW definition described by Preu et al. (2013) for the Argentine Basin: neutral density between 27.90 and 28.10 with a salinity greater than 34.8 PSU. Though this criterion places the UCDW-NADW interface at a slightly deeper level, is also indicates that NADW occupies the deepest portions of the easternmost stations (10–13, Fig. 9b).

5.2 Geostrophic velocity estimates

Based on the observations described in the previous sections, we propose a systematic methodology for estimating geostrophic velocities based on the type of data available. All of the estimates are simple versions of well-established methodologies that can be easily used to monitor the Brazil Current (23 °S–26 °S). In Sections 5.2.1 to 5.2.4, we describe the study cases and present the results. In Section 5.2.5, we discuss the performance of each case and its uncertainties.

5.2.1 VMADCP and CTD profiling

When both VMADCP and CTD profiles are available, geostrophic velocities can be estimated by combining the relative geostrophic velocity with the VMADCP absolute velocity ($v_r = V_{VMADCP}$ in Eq. 1). The method consists of calculating the absolute (barotropic + baroclinic)

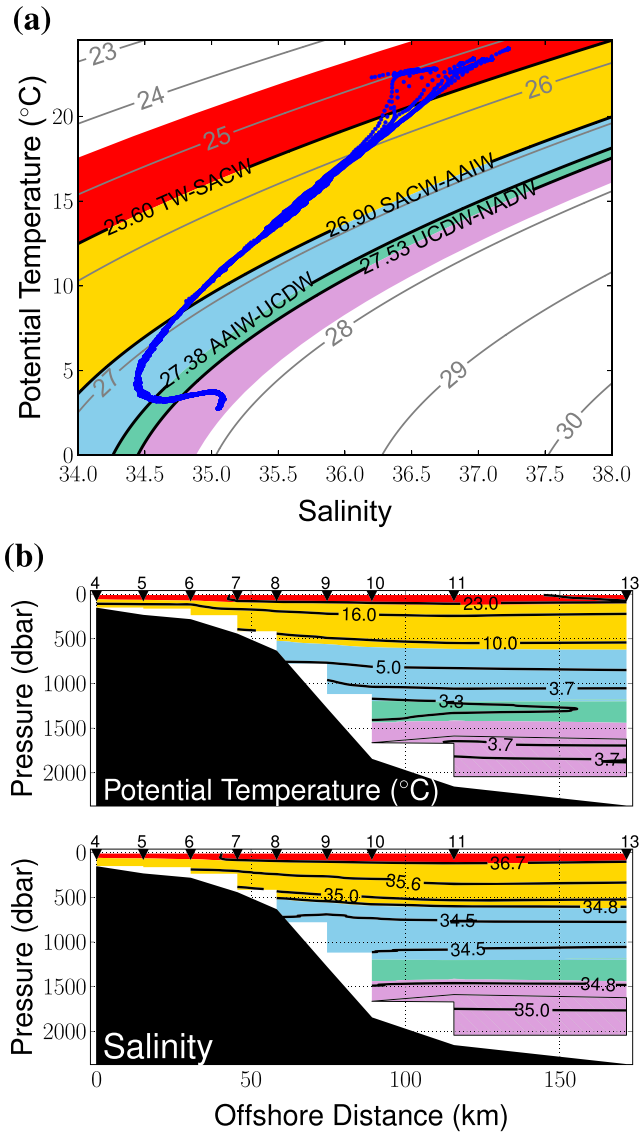

Fig. 9 TS Diagram **a** and potential temperature and salinity sections **b** for the CERES transect. The *color scheme* indicates the observed water masses following the σ_0 interfaces described by (Mémery et al. 2000). The *shaded area* in **b** represents presence of the NADW based on the criterion of (Preu et al. 2013)

geostrophic velocity profile averaged between two CTD stations. This kind of approach has the advantage of not requiring an arbitrarily chosen level of no motion; therefore, the barotropic component is estimated from direct velocity observations. This methodology is based on Pickart and Lindstrom (1994) and Cokelet et al. (1996), who defined how V_{VMADCP} should be applied as v_r. Ideally, we must use the geostrophic component of the V_{VMADCP} as reference. However, VMADCP measures the total velocity in the upper ocean. For a potential v_r, we considered the V_{VMADCP} that obeys two basic criteria: it must be located at a pressure level off the Ekman layer, and it has to be in the equipment's depth range of operation.

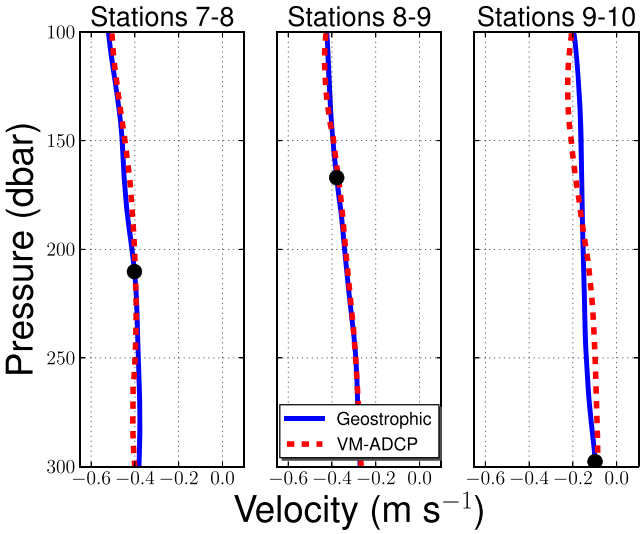

Fig. 10 Absolute geostrophic velocity profiles (*solid blue lines*) and average VMADCP cross-sectional velocity profiles (*dashed red lines*). The *black dots* indicate the reference depths used

To define the first criterion, we computed the mean Ekman layer depth (D_E) within the Santos Basin for the CERES cruise. The estimates were made using sea surface wind from the National Center for Environmental Prediction (NCEP) Reanalysis and AVISO daily wind speed data. We estimated D_E using Eq. 2 Cushman-Roisin B and Beckers JM (1994).

$$D_E = \frac{\gamma}{f_0}\sqrt{\frac{|\tau|}{\rho_0}}, \tag{2}$$

where γ =0.4 is the Von Karman's constant, $|\tau|$ is the magnitude of the wind stress, and ρ_0 is the mean density of the mixed layer observed in the CERES hydrographic transect. The results show that D_E is ~45.6 m (45.9 dbar) and ~35.3 m (35.5 dbar) when calculated from the NCEP and AVISO data, respectively.

From the Ekman theory and assuming a constant eddy viscosity of 0.05 m^2 s^{-1}, the wind-driven current speed at

Table 2 Reference levels employed in the VMADCP-referenced dynamic method

Stations	Offshore distance (km)	Bathmetry (m)	Reference Pressure (dbar)
4-5	8	196	128
5-6	23	325	133
6-7	38	587	172
7-8	52	937	210
8-9	66	1,418	167
9-10	82	1,876	298
10-11	102	2,299	212
11-13	143	2,431	160

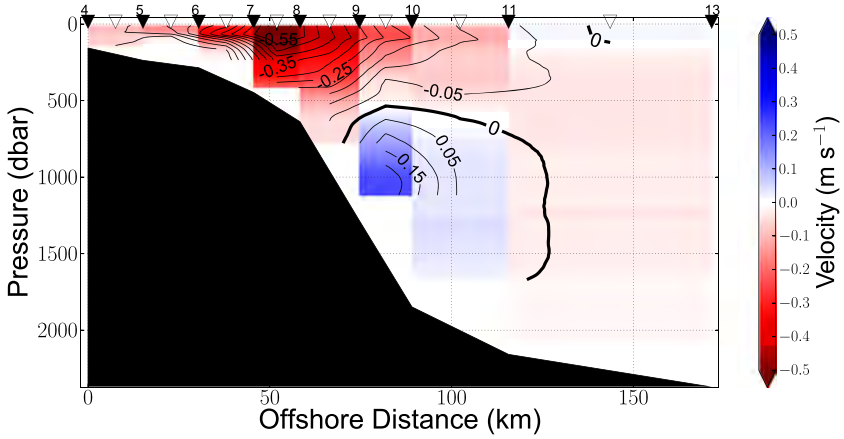

Fig. 11 VMADCP-referenced absolute geostrophic velocity transect. Negative velocities are southwestward, *black triangles* indicate the locations of the stations, and *white triangles* represent the locations of the geostrophic profiles

100 dbar corresponds to ∼7 % of the surface speed (V_E). The value of V_E obtained using the NCEP (AVISO) wind stress is ∼0.024 (0.023) m s^{-1}. Therefore, the BC velocities at 100 dbar are two orders of magnitude higher than the wind-driven current speed at this isobaric level. Because the velocity was measured by a 75 kHz VMADCP, we referenced our calculations between the 100 and 300 dbar pressure levels. This procedure guarantees that both criteria are satisfied.

We spatially averaged the VMADCP cross-sectional velocity profiles between the CTD stations to obtain the mean VMADCP profiles at the same locations as the geostrophic profiles. The reference level was then chosen by matching the VMADCP and relative geostrophic profiles in a least-squares sense. Figure 10 illustrates the reference profiles and the resulting absolute geostrophic velocities at selected station pairs. All of the reference levels employed are presented in Table 2.

The ADCP-referenced geostrophic velocity field is shown in Fig. 11. The BC is depicted as a southwestward flow with maximum surface velocities of approximately -0.60 m s^{-1} (stations 7 and 8) and a volume transport of -6.77 Sv. At stations 8 and 9, the BC appears to extend down to 600 dbar. At intermediate levels, the IWBC signal is restricted to stations 9–11 and extends from 500 dbar to ∼1,700 dbar, yielding a volume transport of 1.02 Sv. The IWBC core is centered at stations 9 and 10 with maximum velocities of approximately 0.24 m s^{-1} at 1,000 dbar.

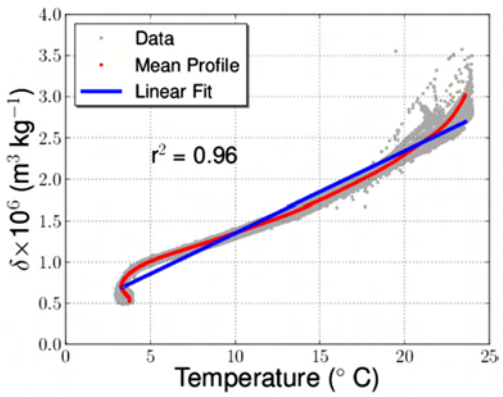

Fig. 12 Linear fit of the climatological temperature-specific volume anomaly (δ) curve in the Santos Basin

5.2.2 VMADCP and temperature (T) profiling

As pointed out in Section 1, vessels equipped with different oceanographic sensors will be operating within the pre-salt reservoir area. These vessels, which cannot stop operating to deploy LADCP or CTD, can also be used to estimate geostrophic velocities.

Based on the relationship between the climatological temperature (**T**) and the specific volume anomaly (δ), we established a form to derive the mass field from only vertical temperature profiles. This kind of approach is useful for data acquired by supply vessels equipped with instruments such as Expendable Bathythermographs (XBTs).

We calculated the mean δ profile from the WOA13 temperature (Locarnini et al. 2013) and salinity (Zweng et al. 2013) data within the study region. Based on this averaged curve, we modeled the relationship between **T** and its associated δ using a linear fit. The model is presented in Fig. 12 and Eq. 3.

$$\delta(\mathrm{T}) = [0.0988\mathrm{T} + 0.3635].10^{-6}. \quad (3)$$

To test Eq. 3, we computed δ from the CERES CTD temperature profiles and the VMADCP-referenced absolute geostrophic velocity. The XBT-like derived geostrophic velocity transect is shown in Fig. 13. The velocity pattern is similar to that obtained in Section 5.2.1, which suggests that the linear fit is a satisfactory model. Note that the BC has maximum velocities of -0.57 m s^{-1} (stations 7 and 8) and a volume transport of -6.55 Sv. At depths greater than 500 dbar, the IWBC flows northeastward with a maximum

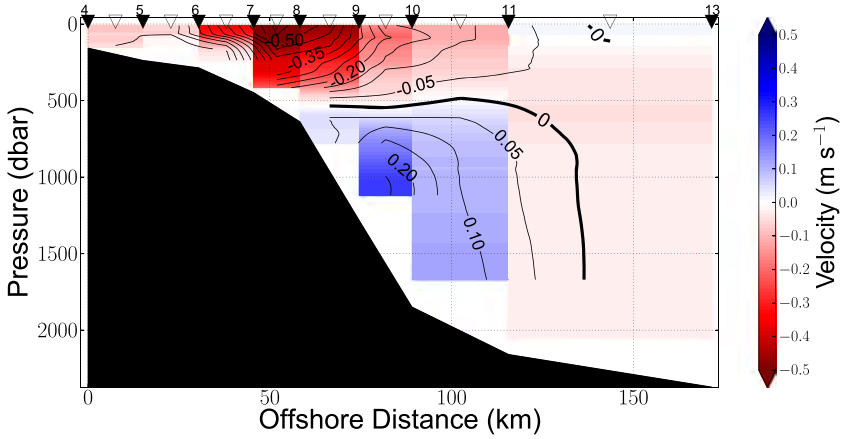

Fig. 13 Similar to Fig. 11 but for the geostrophic velocity derived from only temperature profiles

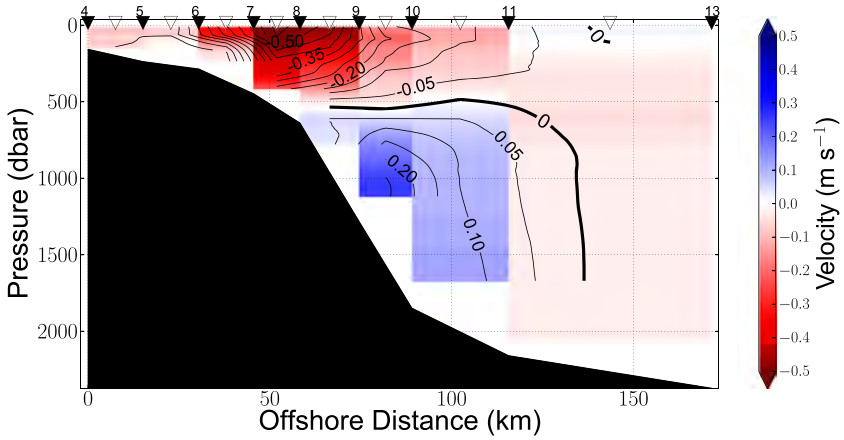

Fig. 14 Isopycnal (26.82 kg m^{-1}, *magenta line*) referenced absolute geostrophic velocity transect. Negative velocities are southwestward, *black triangles* indicate the locations of the stations, and *white triangles* represent the locations of the geostrophic profiles

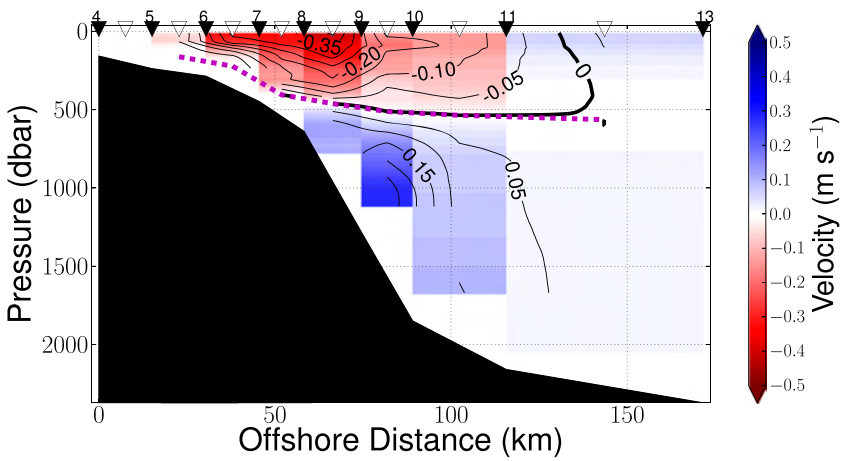

Fig. 15 Similar to Fig. 14 but for the geostrophic velocity derived from only temperature profiles

velocity of ∼0.26 m s^{-1} (stations 9 and 10) and a volume transport of 3.13 Sv. We should emphasize that this calculation differs from that presented in Section 5.2.1 solely by the computation of δ.

5.2.3 CTD profiling

If VMADCP data are not available, absolute geostrophic velocities can be estimated using the isopycnal depth of 26.82 kg m^{-3} as the zero cross-section velocity level (see Section 4). As expected, the mean pressure at the CERES transect that corresponds to the isopycnal 26.82 kg m^{-3} is approximately 500 dbar (Fig. 9).

Figure 14 presents the resulting geostrophic field. Once again, the BC is depicted as having a width of approximately 100 km (stations 5 and 6 to 10 and 11) and a vertical extent of ∼500 dbar. Its maximum surface velocities reach -0.38 m s^{-1} (stations 7 and 8), and the volume transport is -4.07 Sv. The IWBC signal is clear from stations 8-9 to 10-11 and has maximum intensities of 0.26 m s^{-1} (stations 9-10) at ∼1,000 dbar. The volume transport at intermediate depths is 2.72 Sv.

5.2.4 Temperature (T) profiling

Assuming that only temperature profiles are available, absolute geostrophic velocities can be estimated by applying Eq. 3 and the isopycnal level of 26.82 kg m^{-3} as reference (∼500 dbar). Before performing the referencing, the specific volume anomaly (δ) field obtained from Eq. 3 is added to the standard specific volume and used to obtain the potential density (σ_0) field. The results are shown in Fig. 15. Note that both the BC and IWBC have shapes and dimensions that are comparable to those obtained using the other methods. The BC's core is centered at stations 8-9 with maximum surface intensities of approximately -0.41 m s^{-1}, and its volume transport is -4.86 Sv. The IWBC's core is located at ∼1,000 dbar (stations 9-10) and has a maximum velocity of 0.28 m s^{-1} and a volume transport of approximately 3.13 Sv.

5.2.5 Methodology performance and uncertainties

The geostrophic velocity fields obtained in the previous sections (Figs. 11, 13, 14, and 15) are in good qualitative agreement with the directly observed velocity field from LADCP measurements (Fig. 8). To quantify how similar the geostrophic estimates are to the LADCP measurements, we linearly interpolated the LADCP observations to the geostrophic grid and compared the velocity profiles.

Figure 16 shows the absolute difference fields between the geostrophic estimates and the interpolated LADCP profiles. Note that the VMADCP-referenced method (panels a and b) yielded better estimates in the BC current domain (pressures < 500 dbar; stations 5-6 to 10-11) compared to the level of no motion assumption (panels c and d). At the BC's core (stations 7 and 8), the isopycnal method (panel c) underestimated the barotropic component by 0.08–0.24 m s^{-1}, which is clearly due to the fact that the BC occupies the entire water column at stations 7 and 8, and the no motion level is not observed (Fig. 8).

At pressures greater than 500 dbar, the level of no motion assumption performed as well as the VMADCP-referenced methods. This further confirms that the isopycnal level of 26.82 kg m^{-3} (∼500 dbar) can be used as reference. The similar difference distributions (Fig. 16, left and right panels) also indicate that the applied linear relationship between δ and **T** (Eq. 3) is a reasonable first-order approximation.

We plotted the geostrophic profiles closest to the BC and IWBC cores in Fig. 17 with the corresponding interpolated LADCP profiles. As we observed before, the barotropic component from the VMADCP is better represented (see smaller RMS differences in panels a and b) than in the isopycnal methods (panels c and d). Another important aspect is the vertical shear of the LADCP observed velocities; the LADCP shear is similar to the geostrophic shear, in particular outside the ageostrophic area at pressures greater than 100 dbar, which reinforces the applicability of the methods used in this study. As expected, if the geostrophic calculations are properly applied, the BC-IWBC system can be represented accurately.

Finally, we recomputed the LADCP-derived volume transports of the BC and IWBC using the average velocity profiles between two consecutive station locations (linearly interpolated profiles). This simple difference in estimating the transports aimed a more adequate and precise direct comparison between the transports inferred from geostrophy and those calculated from directly observed velocities. The new transport values for the station-pair averaged LADCP of the BC and the IWBC are -5.12±0.88 and 2.01±0.61 Sv, respectively. Table 3 summarizes the geostrophic and LADCP transport estimates. Our four geostrophic estimates yield mean volume transports of -5.56 ±1.31 and 2.50 ±1.01 Sv for the BC and IWBC, respectively. The ranges of the geostrophic volume transports represent the standard deviations of the four values.

Despite the good agreement between the geostrophic estimates and the direct observations, the errors and uncertainties involved in such geostrophic estimates must be considered. Johns et al. (1989) stated that the overall error in the geostrophic velocity (dv_g) can be estimated by assuming three primary sources of uncorrelated errors (Eq. 4).

$$dv_g = \sqrt{(\frac{d\Delta D}{fL})^2 + (\frac{dL}{L}v_g)^2 + (dv_r)^2}. \quad (4)$$

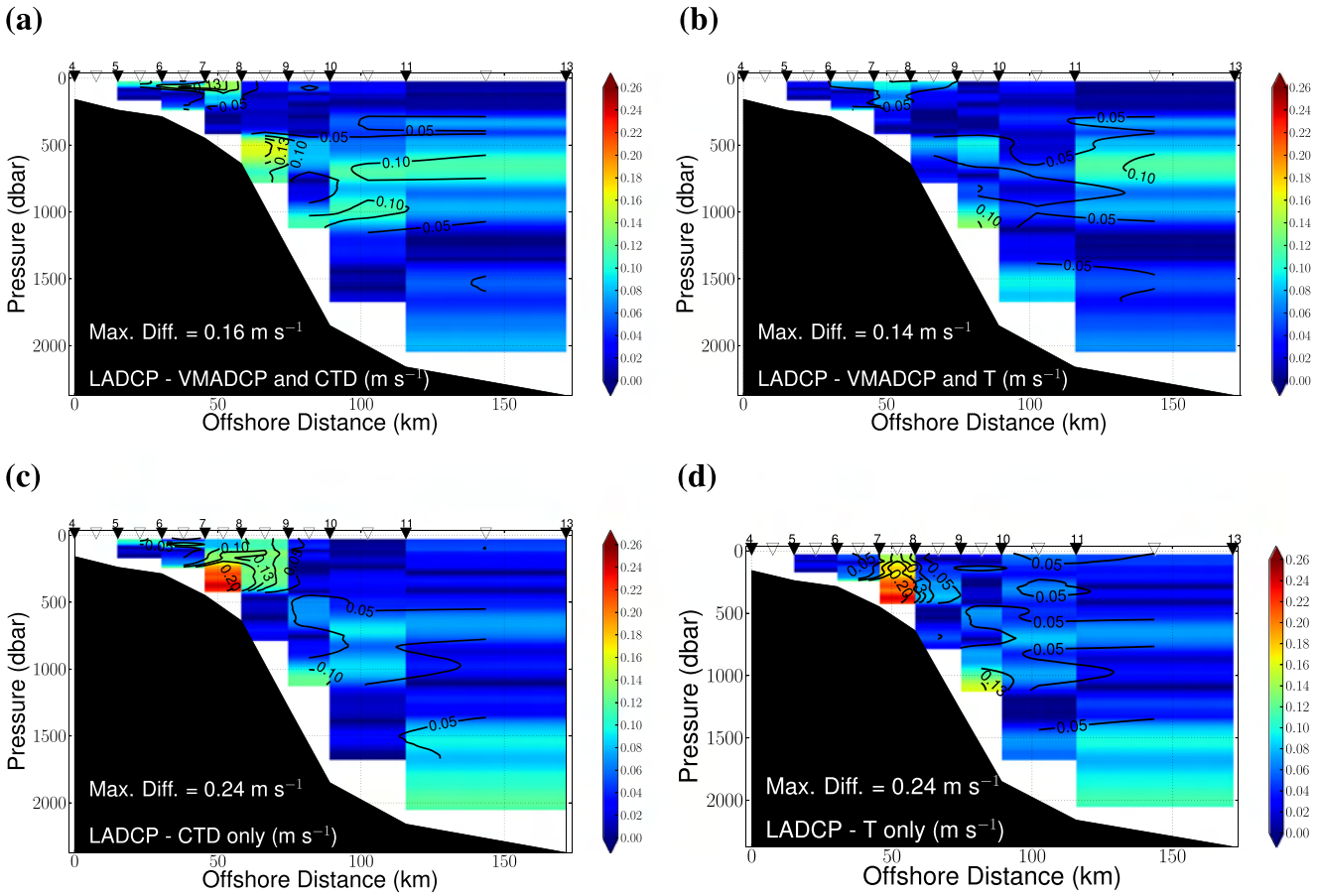

Fig. 16 Absolute difference distributions between the LADCP and the geostrophic velocities from **a** VMADCP and CTD, **b** VMADCP and T, **c** CTD only and **d** T only. *Black triangles* indicate the locations of the stations, and *white triangles* represent the locations of the velocity profiles

We now examine Eq. 4 by evaluating each of the three terms on the right hand side. The first term is related to the dynamic height anomaly (ΔD), or $\int_p^{p_r} \delta dp'$, and is based on the measurement errors in temperature and salinity. The second term is the station spacing (L) term and is due to the uncertainties in the station spacing (dL). The last term is related to the accuracy of the reference velocity (dv_r). It is important to note that the expression for dv_g assumes L to be adequate for resolving the BC and IWBC flows. Such a mesoscale and geostrophic current system, with one velocity reversal in the water column, can be described using the first-order Rossby deformation radius as the scale for L (e.g., Cushman-Roisin and Beckers, 1994. Based on climatological (WOA13) and in situ data (CERES), the first deformation radius is ∼23 km. The station spacing is approximately 15 km except for stations 10-11 and 11-13, which have spacings of 26 and 55 km, respectively. Because a 55 km spacing does not allow for a proper evaluation of the geostrophic velocity vertical shear, no error analysis and considerations were performed for the geostrophic profiles at stations 11–13.

With the dynamic heights determined to an accuracy of 0.04 m^2 s^{-2} by Johns et al. (1989), we were able to estimate the term $dD = |\frac{d\Delta D}{fL}|$. Because the precision of CTDs has evolved over the last 20 years and considerable advances have been made in the estimates of seawater properties, $d\Delta D$ of 0.04 m^2 s^{-2} represents a conservative value. The presented geostrophic calculations using CTD profiling yield dD values of approximately 0.04 m s^{-1} in profiles 4-5 to 9-10 and 0.02 m s^{-1} at stations 10–11. If only temperature profiles are available, we proposed a linear relationship to estimate the specific volume anomaly, which makes the error assessment more difficult. This procedure considerably increases $d\Delta D$, especially in the water column layers in which the salinity is important for density variations (see Fig. 9). As described before, the linear relationship is a good first approximation, and the intent is to propose a useful tool to perform a first assessment of the BC-IWBC's geostrophic pattern from data such as XBT transects. The associated error must be better evaluated in terms of the accuracy of the sensors and the methods approximation.

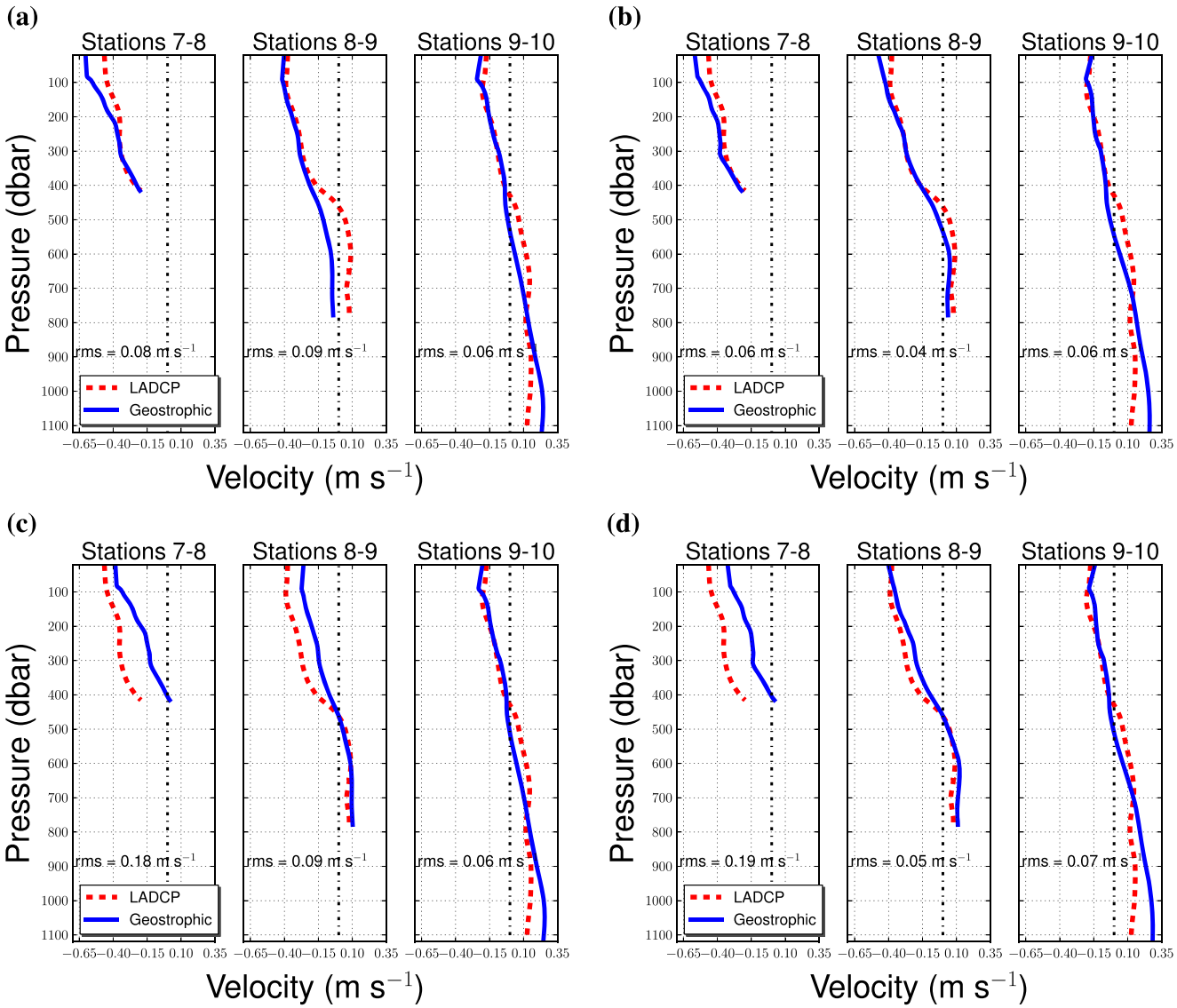

Fig. 17 LADCP and geostrophic profiles at the cores of the BC and IWBC. The geostrophic profiles are from **a** VMADCP and CTD, **b** VMADCP and T, **c** CTD only, **d** T only data

The station spacing term is similar in all of the applied methods. The primary factor that impacts the accuracy of dL is the ship drift during a CTD cast (Johns et al. 1989).

Table 3 Volume transports (Sv) of the BC-IWBC System over the geostrophic field area

	BC	IWBC
LADCP	-5.12 ±0.88	2.01 ±0.64
VMADCP and CTD profiles	-6.77	1.02
VMADCP and T Profiles	-6.55	3.13
Only CTD profiles	-4.07	2.72
Only T profiles	-4.86	3.13
Geostrophic mean values	-5.56 ±1.31	2.50 ±1.01

The mean drift recorded is 1.02 km (maximum drift=1.1 km at station 13), so we considered a mean spacing error of $dL = \sqrt{1.02^2 + 1.02^2} \approx 1.44$ km. In all of the geostrophic methods, this term will be greatest in the BC core region (stations 7 and 8) and less elsewhere. Because the highest magnitude of the geostrophic BC was 0.6 m s^{-1} from the VMADCP-referenced method, the maximum $|\frac{dL}{L} v_g|$ is approximately 0.06 m s^{-1}.

Finally, we can estimate the reference velocity term ($|dV_r|$). Arbitrary assumptions of the level of no motion can also make the estimation of dV_r arbitrary. In this case, we should be able to evaluate the temporal and spatial variability of the 26.82 kg m^{-3} isopycnal or the level of no motion within the Santos Basin. The 1-year velocity time series from the COROAS mooring only provides the

temporal variability over the 1,000-m isobath, so a rough estimate of dV_r can be made by using the velocity's standard deviation (0.002 m s^{-1}) from the mooring's level of no motion time series. When VMADCP is used as reference, the error is easier to evaluate. Meinen et al. (2000) showed that in this approach, dV_r basically depends on the ageostrophic velocity components in the reference velocity signal. Because barotropic and baroclinic tides reach maximum velocities of a few centimeters per second in the BC-IWBC domain (e.g., Palma et al. 2004 and Pereira et al. 2007), and the BC-IWBC signal in direct velocity measurements is mostly geostrophic (see Fig. 17), we can use the VMADCP accuracy of 0.03 m s^{-1} (e.g., Schott et al. 2005) as a conservative error estimate.

Now, we can estimate the left hand side of Eq. 4. Considering the error highest values described above, dv_g is approximately 0.08 and 0.07 m s^{-1} for VMADCP-referenced and isopycnal methods in the BC core region, respectively. We should emphasize again that the linear fit used to estimate the specific volume anomaly increases the error and it must be better evaluated.

6 Summary and conclusions

Systematic and simple methodologies to estimate the geostrophic velocities in the BC-IWBC domain (23 °S–26 °S) are proposed based on the type of data available, including (i) VMADCP and CTD profiles, (ii) VMADCP and temperature profiles, (iii) only CTD profiles, and (iv) only temperature profiles.

When VMADCP data are not available (iii and iv), a level of no motion is considered as reference. Therefore, we first evaluated the applicability of this assumption by comparing currentmeter data with three hydrographic transects. We concluded that the isopycnal level of 26.82 kg m^{-3} (∼500 dbar), which lies close to the SACW/AAIW interface, can be applied as the level of no motion in the study region (Section 4).

The performance of methods (i)–(iv) was evaluated by comparing geostrophy to LADCP top–bottom measured velocities in terms of the current dimensions, position in the transect, shape, volume transport, and maximum speed (Section 5). The LADCP transect revealed a parabola-shaped BC that flows southwestward over the continental shelf-break and slope and has a width of ∼100 km and a vertical extent of 500 m. Its core has maximum velocities of approximately -0.59 m s^{-1} and a volume transport of -5.75 ± 1.53 Sv. The IWBC is depicted as an elliptically-shaped undercurrent that flows northeastward near the continental slope. Its vertical extent and width are ∼1,300 m and ∼60 km, respectively. The IWBC has maximum velocities of approximately 0.22 m s^{-1} and a volume transport of 4.11 ± 2.01 Sv.

Despite the large uncertainties involved in the geostrophic calculations, all of the proposed methods agree well with the directly observed velocity field. Our geostrophic transport estimates are -5.56 ±1.31 and 2.50 ±1.01 Sv for the BC and IWBC, respectively. The performance analysis indicates that the VMADCP-referenced method better estimated the barotropic velocity component in regions shallower than 500 m. Another important conclusion is that a linear relationship between the temperature and the specific volume anomaly can be used to perform a first assessment of the BC-IWBC system from XBT-like data sets.

It is important to stress that all of the methods (i–iv) are simple versions of well-established methodologies and that they all can be refined and combined with other methodologies to yield more reliable estimates. However, we believe that the simplicity presented in this study and the intense oil industry activities in the area can provide unprecedented data coverage of the BC-IWBC system and may be used to establish a monitoring system.

Acknowledgements We acknowledge the Brazilian National oil company PETROBRAS for the CERES experiment data set and their partnership. We also acknowledge the two anonymous reviewers and MSc. César Barbedo Rocha for thoughtful insights and important suggestions. This research was funded by Séo Paulo Research Foundation (FAPESP, 2012/05221-2 and 2013/10475-6). Ilson Carlos Almeida da Silveira and Belmiro Mendes de Castro acknowledge support from CNPq (307122/2010-7).

References

Boebel O, Davis RE, Ollitrault M, Peterson RG, Richardson PL, Schmid C, Zenk W (1999) The intermediate depth circulation of the western south atlantic. Geophys Res Lett 26(21):3329–3332

Campos EJD, Gonçalves JE, Ikeda Y (1995) Water mass characteristics and geostrophic circulation in the South Brazil Bight: Summer of 1991. J Geophys Res 1lo(C9):18, 537–18,550

Campos EJD, Ikeda Y, Castro BM, Gaeta SA, Lorenzzetti JA, Stevenson MR (1996) Experiment studies circulation in the western south atlantic. EOS, Trans Am Geophys Union 77(27):253–264

Carminatti M, Wolff B, Gamboa LAP (2008) New exploratory frontiers in Brazil, In: 19th World Petroleum Congress. Madrid, Spain

Cokelet ED, Shcall ML, Dougherty DM (1996) ADCP-Referenced geostrophic circulation in the bering sea basin. J Phys Oceanogr 26(7):1113–1128

Cushman-Roisin B, Beckers JM (1994). In: 2nd (ed) Introduction to geophysical fluid dynamics: Physical and numerical aspects, international geophysics series, Vol 101. Elsevier

Duarte CSL, Viana AR (2007) Santos drift system: Stratigraphic organization and implications for late Cenozoic paleocirculation in the Santos Basin, SW Atlantic Ocean. Geological Society, London. Special Publications 276:171–198

Emery WJ, Thomson RE (2001) Data analysis methods in physical oceanography. Elsevier, Amsterdam, The Netherlands

Evans DL, Signorini SR (1985) Vertical structure of the Brazill Current. Nature 315:48–50

Evans DL, Signorini SR, Miranda LB (1983) A note on the transport of the Brazil Current. J Phys Oceanogr 13(9):1732–1738

Fischer J, Visbeck M (1993) Deep velocity profiling with self-contained ADCPs. J Atmos Oc Tech 10:764–773

Garfield N (1990) The Brazil Current at subtropical latitudes, PhD thesis. University of Rhode Island, Rhode Island

Johns E, Watts RD, Rossby TH (1989) A Test of geostrophy in the gulf stream. J Phys Oceanogr 94(C3):3211–3222

Legeais JF, Ollitrault M, Arhan M (2013) Lagrangian observations in the Intermediate Western Boundary Current of the South Atlantic. Deep-Sea Res II(85):109–126

Lima JAM (1997) Oceanic circulation on the Brazil Current shelf break and slope at 22 sS, PhD thesis, publisher=University of New South Wales, address=New South Wales

Locarnini RA, Mishonov AV, Antonov JI, Boyer TP, Garcia HE, Baranova OK, Zweng MM, Paver CR, Reagan JR, Johnson DR, Hamilton M, Seidov D (2013) World Ocean Atlas 2013, Volume 1: Temperature. Tech. rep., NOAA Atlas NESDIS 73

Meinen CS, Watts RD, Clarke AR (2000) Absolutely referenced geostrophic velocity and transport on a section across the North Atlantic Current. Deep-Sea Res I: Oceanogr Res Pap 47:309–322

Meinen CS, Piola AR, Perez RC, Garzoli SL (2012) Deep Western Boundary Current transport variability in the South Antlantic: Preliminary results from a pilot array at 34.5 °S. Ocean Sci 8:1041–1054

Meisling KE, Cobbold PR, Mount VS (2001) Segmentation of an obliquely-rifted margin. AAPG Bulletin 85(11):1903–1924

Mémery L, Arhan M, Alvarez-Salgado XA, Messias MJ, Mercier H, Castro CG, Rios AF (2000) The water masses along the western boundary of the south and equatorial Atlantic. Prog Oceanog 47(1):69–98

Miranda LB, Filho BMC (1979) Condições do movimento geostrófico das águas adjacentes a Cabo Frio (RJ). BOL DO INST OCEANOGR 28(2):79–93

Mohriak WU, Nóbrega M, Odegard ME, Gomes BS, Dickson WG (2010) Petr Geosc 16:231–245

Müller TJ, Ikeda Y, Zangenberg N, Nonato LV (1998) Direct measurements of western boundary currents off brazil between 20°S and 28°S. J Geophys Res 103(C3):5429–5437

Palma ED, Matano RP, Piola AR (2004) A numerical study of the Southwestern Atlantic Shelf circulation: Barotropic response to tidal and wind forcing. J Geophys Res 109(C08–104)

Pereira AF, Castro BM, Calado L, Silveira ICA (2007) Numerical simulation of M_2 internal tides in South Brazil Bight and their interaction with the Brazil Current. J Geophys Res 112(C04009)

Pickart RS, Lindstrom SS (1994) A comparison of techniques for referencing geostrophic velocities. J Atmos Oc Tech 11(3):814–824

Preu B, Hernódez-Molina FJ, Violante R, Piola AR, Paterlinif CM, Schwenk T, Voigt I, Krastel S, Spiess V (2013) Morphosedimentary and hydrographic features of the northern Argentine margin: the interplay between erosive, depositional and gravitational processes and its conceptual implications. Deep-Sea Res I: Oceanogr Res Pap 75:157–174

Rocha CB, da Silveira ICA, Castro BM, Lima JAM (2014) Vertical structure, energetics, and dynamics of the Brazil Current System at 22 °S–28 °S. J Geophys Res-Oceans 19(1):52–69

Schott FA, Dengler M, Zantopp R, Stramma L, Fischer J, Brandt P (2005) The shallow and deep western boundary circulation of the south atlantic at 5°–11 °S. J Phys Oceanogr 35:2031–2053

Signorini SR (1978) On the circulation and the volume transport of the Brazil Current between the Cape of São Tomé and Guanabara Bay. Deep-Sea Res 5(25):481–490

Silveira IC, Lima JAM, Schimdt ACK, Ceccopieri W, Satori A, Francisco CPF, Fontes RFC (2008) Is the meander growth in the Brazil Current System off Southeast Brazil due to baroclinic instability? Dynam Atmos Oceans 45:187–207

Silveira ICA, Schimidt ACK, Campos EJD (2001) A Corrente do Brasil ao largo da costa leste brasileira. R bras Oceanogr 48(2):171–183

Silveira ICA, Calado L, De Castro BM, Cirano M, Lima JAM, Mascarenhas AS (2004) On the Baroclinic structure of the Brazil Current-Intermediate Western Boundary Current at 22°–23°. S. Geophys Res Lett 31:4308

Stramma L (1989) The Brazil Current transport south of 23 °S. Deep-Sea Res 36(4A):639–646

Stramma L, England M (1999) On the wather masses and mean circulation of the South Atlantic Ocean. J Geophys Res 104(C9):20, 863–20, 883

Stramma L, Fischer J, Reppin J (1995) The North Brazil undercurrent. Deep-Sea Res I: Oceanogr Res Pap 42(5):773–795

Vianna ML, Menezes VV (2011) Double-celled subtropical gyre in the South Atlantic Ocean: Means, trends and interannual changes. J Geophys Res 116(C03–s024)

Visbeck M (2002) Deep velocity using acoustic doppler current profilers: botton track and inverse solutions. J Atmos Oc Tech 19:794–807

Zembruscki S (1979) Geomorfologia da Margem Continental Sul Brasileira e das Bacias Ocenicas Adjacentes. In Projeto REMAC. PETROBRAS. CEMPES. DINTEP (Série REMAC $n°$ 7), pp 129–177

Zweng MM, Reagan JR, Antonov JI, Locarnini RA, Mishonov AV, Boyer TP, Garcia HE, Baranova OK, Johnson DR, Seidov D, Biddle MM (2013) World ocean atlas 2013, Volume 2: Salinity. Tech. rep., NOAA Atlas NESDIS 73